

# Two-dimensional demonstration of Wigner phase-retrieval microscopy in the STEM configuration

B.C. McCallum and J.M. Rodenburg

*Cavendish Laboratory, University of Cambridge, Madingley Road, Cambridge CB3 0HE, UK*

Received 30 March 1992; in revised form 15 June 1992

Following earlier work [S.L. Friedman and J.M. Rodenburg, *J. Phys. D* 25 (1992) 147] which has shown, using light optics in one dimension, that a poor lens of limited aperture (such as that encountered in both electron and X-ray microscopy) need not limit spatial resolution, we present here experimental proof that the method can be straightforwardly extended to two-dimensional images. We employ a scanning optical microscope in the configuration of the scanning transmission electron microscope (STEM) to solve for the specimen structure at “super-resolution” for (1) a two-dimensional magnitude specimen, (2) an extended two-dimensional magnitude specimen and (3) a pure strong-phase specimen.

## 1. Introduction

It has long been known that the microdiffraction plane of a scanning transmission electron microscope (STEM) is a complex mixture of diffraction [1], shadow-image [2], and holographic [3,4] information. Furthermore, when any point in the microdiffraction plane is collected as a function of probe position, it contains all the conventional bright and dark-field image information, depending on where the chosen detection point lies relative to the optic axis. Bates and Rodenburg [5] have shown that (at least when working within the projection approximation) the instrument and specimen contributions can be separated by a simple deconvolution using a Wigner distribution if all of this data is collected in one experiment. Not only does this remove the influences of any aberrations or defocus in the lens, it also retrieves the phase of the wavefield on the exit surface of the specimen (at least within the projection approximation) and therefore offers the opportunity of providing a super-resolution estimate of the specimen in complex amplitude, without being limited to the weak-phase approxi-

ation, and without requiring a stable holographic reference wave. The phase-retrieval process is most appropriately performed in the diffraction plane [6], for it then also allows the reconstruction to exceed the conventional “information limit” of the microscope, which in electron microscopy is usually dominated by instrument instability, chromatic spread and the incoherence terms which arise from the finite source and detector sizes (as opposed to a physical objective aperture).

Qualitatively, we may think of the method in terms of reciprocity [7] as follows. Any one image recorded with tilted illumination in a conventional transmission electron microscope will have a certain range of spatial frequencies present, this range being limited by the aperture or envelope function lying in the back focal plane of the objective lens. Different illumination tilt angles will pass different regions of the diffraction pattern through the central, good-quality part of the transfer function. Of course, no single image will give an unambiguous estimate of the phase of the wavefield because of the usual limitations of the transfer function. However, by using the entire

data set (all images as a function of the illumination tilt angles), the relative phase between each pair of points in the diffraction pattern can be inferred from the absolute position (and the changes in their position as a function of tilt) of their corresponding interference fringes in the image plane. Having accounted for the phase of the transfer function via the deconvolution, the process can thus provide an estimate of the relative phase between any two points in reciprocal space which are separated by less than the stable width of the objective aperture function. Consequently, it is possible to build up an aperture, in theory of unlimited size, in a way which is closely akin to aperture-synthesis in radio astronomy. We refer to the method as “Wigner phase-retrieval microscopy” (WPM) to emphasise both the phase-sensitive nature of the reconstruction and the fact that the crucial deconvolution occurs in a Wigner distribution, which is a mixture of both real space and reciprocal space coordinates. In practice, because such a closely sampled set of illumination conditions is difficult to obtain in the conventional transmission microscope, we formulate the theory and perform the experiments in the STEM mode, where such data can simultaneously be recorded for each image pixel (defined as the position of the focused-probe crossover).

WPM is described in section 2, and the two-dimensional (2D) optical STEM analogue used to collect WPM data for subsequent processing is described in section 3. In section 4, we present results showing the reconstruction of a 2D finite-sized magnitude specimen. However, any actual STEM specimen is typically many orders of magnitude larger than the region of interest. In section 5, we show that it is theoretically possible to reconstruct the specimen function over a small region of a large specimen, by appropriately windowing the microdiffraction data that is recorded as the probe is scanned over that region. Results are then presented of the application of this method to the reconstruction of an extended object. Furthermore, one is often interested in phase-only specimens. This poses no problem theoretically, since WPM is capable of recovering the complex amplitude of the specimen function.

In section 6, we show that it is indeed possible to reconstruct a phase-only specimen function from measured microdiffraction data. Finally, conclusions are drawn in section 7.

## 2. Theory

It is first necessary to describe WPM as applied in STEM [5,6]. The complex specimen and probe functions are denoted by  $\psi(\mathbf{r})$  and  $a(\mathbf{r})$ , respectively (where  $\mathbf{r}$  is a coordinate in 2D real space), and the position of the probe with respect to the specimen by  $\boldsymbol{\rho}$ . The reciprocal space coordinates corresponding to  $\mathbf{r}$  and  $\boldsymbol{\rho}$  are denoted by  $\mathbf{r}'$  and  $\boldsymbol{\rho}'$ , respectively, and the Fourier transforms of  $\psi(\mathbf{r})$  and  $a(\mathbf{r})$  by  $\Psi(\mathbf{r}')$  and  $A(\mathbf{r}')$ . Note that elsewhere [5] we referred to the probe function as  $p(\mathbf{r})$ ; however, we adopt  $a(\mathbf{r})$  here to emphasise its Fourier relationship to the objective aperture function  $A(\mathbf{r}')$ . The complex amplitude  $M(\mathbf{r}', \boldsymbol{\rho})$  in the microdiffraction plane is simply

$$\begin{aligned} M(\mathbf{r}', \boldsymbol{\rho}) &= \text{FT}_{\mathbf{r}}\{a(\mathbf{r} - \boldsymbol{\rho})\psi(\mathbf{r})\} \\ &= \int a(\mathbf{r} - \boldsymbol{\rho})\psi(\mathbf{r}) \exp(i2\pi\mathbf{r} \cdot \mathbf{r}') \, d\mathbf{r}, \end{aligned} \quad (1)$$

where  $\text{FT}_{\mathbf{r}}\{\}$  denotes a Fourier transformation with respect to the  $\mathbf{r}$  coordinate only. By the convolution theorem,  $M(\mathbf{r}', \boldsymbol{\rho})$  can also be expressed as

$$\begin{aligned} M(\mathbf{r}', \boldsymbol{\rho}) &= \text{FT}_{\mathbf{r}}\{a(\mathbf{r} - \boldsymbol{\rho})\} \otimes_{\mathbf{r}'} \text{FT}_{\mathbf{r}}\{\psi(\mathbf{r})\} \\ &= \int A(\mathbf{b}')\Psi(\mathbf{r}' - \mathbf{b}') \\ &\quad \times \exp(i2\pi\boldsymbol{\rho} \cdot \mathbf{b}') \, d\mathbf{b}', \end{aligned} \quad (2)$$

where  $\otimes$  denotes convolution, the subscript indicating the variable(s) over which the convolution is performed.

In practice, only the intensity in the microdiffraction plane (i.e.  $|M(\mathbf{r}', \boldsymbol{\rho})|^2$ ) can be measured, which can be expressed in various different

forms. From eq. (1),  $|M(\mathbf{r}', \boldsymbol{\rho})|^2$  can be expressed in terms of real space quantities as

$$\begin{aligned} |M(\mathbf{r}', \boldsymbol{\rho})|^2 &= M(\mathbf{r}', \boldsymbol{\rho})M^*(\mathbf{r}', \boldsymbol{\rho}) \\ &= \int \int A(\mathbf{b} - \boldsymbol{\rho})\psi(\mathbf{b})a^*(\mathbf{c} - \boldsymbol{\rho})\psi^*(\mathbf{c}) \\ &\quad \times \exp[i2\pi\mathbf{r}' \cdot (\mathbf{b} - \mathbf{c})] d\mathbf{b} d\mathbf{c}, \end{aligned} \quad (3)$$

where \* denotes complex conjugation. Alternatively,  $|M(\mathbf{r}', \boldsymbol{\rho})|^2$  can be expressed in terms of reciprocal space quantities from eq. (2) as

$$\begin{aligned} |M(\mathbf{r}', \boldsymbol{\rho})|^2 &= \int \int A(\mathbf{b}')\Psi(\mathbf{r}' - \mathbf{b}')A^*(\mathbf{c}')\Psi^*(\mathbf{r}' - \mathbf{c}') \\ &\quad \times \exp[i2\pi\boldsymbol{\rho} \cdot (\mathbf{b}' - \mathbf{c}')] d\mathbf{b}' d\mathbf{c}'. \end{aligned} \quad (4)$$

This expression is in the form derived by Cowley [1], except that the probe position  $\boldsymbol{\rho}$  has been explicitly included, and in this form can be thought of as a phase ramp across the aperture function. Yet another possibility is to express  $|M(\mathbf{r}', \boldsymbol{\rho})|^2$  in terms of both real and reciprocal space quantities, by combining eqs. (1) and (2) to give

$$\begin{aligned} |M(\mathbf{r}', \boldsymbol{\rho})|^2 &= \int \int A(\mathbf{b}') \\ &\quad \times \exp(i2\pi\boldsymbol{\rho} \cdot \mathbf{b}')\Psi(\mathbf{r}' - \mathbf{b}')a^*(\mathbf{c} - \boldsymbol{\rho})\psi^*(\mathbf{c}) \\ &\quad \times \exp(-i2\pi\mathbf{c} \cdot \mathbf{r}') d\mathbf{b}' d\mathbf{c} \\ &= \int \int a^*(\mathbf{c} - \boldsymbol{\rho})A(\mathbf{b}') \exp[-i2\pi(\mathbf{c} - \boldsymbol{\rho}) \cdot \mathbf{b}'] \\ &\quad \times \psi^*(\mathbf{c})\Psi(\mathbf{r}' - \mathbf{b}') \\ &\quad \times \exp[i2\pi\mathbf{c} \cdot (\mathbf{b}' - \mathbf{r}')] d\mathbf{b}' d\mathbf{c} \\ &= [a^*(-\boldsymbol{\rho})A(\mathbf{r}')] \\ &\quad \times \exp(i2\pi\boldsymbol{\rho} \cdot \mathbf{r}') \otimes_{\mathbf{r}', \boldsymbol{\rho}} [\psi^*(\boldsymbol{\rho})\Psi(\mathbf{r}')] \\ &\quad \times \exp(-i2\pi\boldsymbol{\rho} \cdot \mathbf{r}')] \end{aligned} \quad (5)$$

The significance of eq. (5) is that  $|M(\mathbf{r}', \boldsymbol{\rho})|^2$  is now separated into two parts, one depending only on the probe function and the other depending only on the specimen function. It is thus possible in principle to remove the effect of the objective

lens by deconvolving  $a^*(-\boldsymbol{\rho}')A(\mathbf{r}') \exp(i2\pi\boldsymbol{\rho} \cdot \mathbf{r}')$  from  $|M(\mathbf{r}', \boldsymbol{\rho})|^2$ . However, the division implicit in any such deconvolution procedure must be performed in  $(\mathbf{r}, \boldsymbol{\rho}')$  space, for it is in this space in which we have a product of two functions, one depending on the specimen and the other on the probe. Specifically, Fourier transformation of  $|M(\mathbf{r}', \boldsymbol{\rho})|^2$  with respect to both  $\mathbf{r}'$  and  $\boldsymbol{\rho}$  yields a quantity we call  $H(\mathbf{r}, \boldsymbol{\rho}')$ , given by

$$\begin{aligned} H(\mathbf{r}, \boldsymbol{\rho}') &= \text{FT}_{-\mathbf{r}', \boldsymbol{\rho}}\{|M(\mathbf{r}', \boldsymbol{\rho})|^2\} \\ &= \chi_a(\mathbf{r}, -\boldsymbol{\rho}')\chi_\psi(\mathbf{r}, \boldsymbol{\rho}'), \end{aligned} \quad (6)$$

where  $\chi_a(\mathbf{r}, -\boldsymbol{\rho}')$  and  $\chi_\psi(\mathbf{r}, \boldsymbol{\rho}')$  are defined by

$$\chi_a(\mathbf{r}, \boldsymbol{\rho}') = \int q^*(\mathbf{c})q(\mathbf{c} + \mathbf{r}) \exp(i2\pi\mathbf{c} \cdot \boldsymbol{\rho}') d\mathbf{c}. \quad (7)$$

Note that  $\chi_a(\mathbf{r}, \boldsymbol{\rho}')$  has the form of a Wigner distribution [8]. Given  $a(\mathbf{r})$ ,  $\chi_a(\mathbf{r}, -\boldsymbol{\rho}')$  can be straightforwardly evaluated by eq. (7) and then removed from  $H(\mathbf{r}, \boldsymbol{\rho}')$  by a suitable deconvolution method (such as a Wiener filter [9]), giving  $\widehat{\chi}_\psi(\mathbf{r}, \boldsymbol{\rho}')$  (where  $\widehat{\phantom{x}}$  is used to denote an estimate of a quantity).

From eq. (6), it follows that  $\widehat{\chi}_\psi(\mathbf{r}, \boldsymbol{\rho}')$  can only be determined in regions of  $(\mathbf{r}, \boldsymbol{\rho}')$  space where  $\chi_a(\mathbf{r}, -\boldsymbol{\rho}')$  has a significant value. If  $a(\mathbf{r})$  is formed from an objective aperture of diameter  $2\alpha$ , then it can be seen from eq. (7) that  $\chi_a(\mathbf{r}, -\boldsymbol{\rho}') = 0$  for  $\|\boldsymbol{\rho}'\| > 2\alpha$ . We shall refer to the circle  $\|\boldsymbol{\rho}'\| = 2\alpha$  as “the  $\boldsymbol{\rho}'$  cutoff”. In this case,  $\widehat{\chi}_\psi(\mathbf{r}, \boldsymbol{\rho}')$  can then only be estimated for values of  $\boldsymbol{\rho}'$  lying within the  $\boldsymbol{\rho}'$  cutoff. To see how the specimen function may be recovered from  $\widehat{\chi}_\psi(\mathbf{r}, \boldsymbol{\rho}')$ , consider the quantity  $D(\mathbf{r}', \boldsymbol{\rho}')$ , as defined by

$$\begin{aligned} D(\mathbf{r}', \boldsymbol{\rho}') &= \text{FT}_{\mathbf{r}}\{\chi_\psi(\mathbf{r}, \boldsymbol{\rho}')\} \\ &= \Psi(\mathbf{r}')\Psi^*(\mathbf{r}' - \boldsymbol{\rho}'). \end{aligned} \quad (8)$$

An estimate of  $\Psi(\boldsymbol{\rho}')$  (note that  $\Psi(\mathbf{r}')$  and  $\Psi(\boldsymbol{\rho}')$  are used interchangeably, since  $\mathbf{r}'$  and  $\boldsymbol{\rho}'$  are both reciprocal space variables) can thus be obtained from  $\widehat{D}(\mathbf{r}', \boldsymbol{\rho}')$  by

$$\widehat{\Psi}(\boldsymbol{\rho}') = \widehat{D}^*(\mathbf{0}, -\boldsymbol{\rho}') / \sqrt{\widehat{D}(\mathbf{0}, \mathbf{0})}, \quad (9)$$

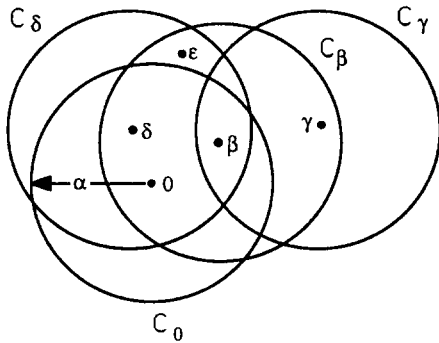


Fig. 1. The  $\rho'$  plane in which  $\widehat{\Psi}(\rho')$  is reconstructed, indicating how  $\widehat{\Psi}(\rho')$  can be obtained outside the  $\rho'$  cutoff.

from which an estimate of the specimen function  $\widehat{\psi}(\rho)$  can be obtained by inverse Fourier transformation. Since  $\widehat{D}(r', \rho') = 0$  beyond the  $\rho'$  cutoff, eq. (9) can only recover  $\widehat{\Psi}(\rho')$  up to the  $\rho'$  cutoff. It should be pointed out that  $\widehat{\psi}(\rho)$ , as well as being recovered in complex amplitude, is recovered to twice the resolution of the bright-field image. This follows since the bright-field image is  $|M(\mathbf{0}, \rho)|^2 = |\text{FT}_{-\rho}\{\Psi(\rho')A(\rho')\}|^2$ , and so only contains information about  $\psi(\rho)$  for  $\|\rho'\| < \alpha$ .

However, the range of  $\rho'$  over which  $\widehat{\Psi}(\rho')$  is recovered can be extended by further consideration of eq. (8). By setting  $r' = \beta$ , where  $\beta$  is some value for which  $\widehat{\Psi}(\beta)$  is already known, it can be seen that  $\widehat{\Psi}(\rho')$  may be recovered over the region  $\|\rho' - \beta\| < \alpha$ . By doing so for various  $\beta$ ,  $\widehat{\Psi}(\rho')$  can in principle be recovered to arbitrarily large  $\|\rho'\|$ . This is now illustrated in detail with the aid of fig. 1, which depicts the plane in which  $\widehat{\Psi}(\rho')$  exists. Data from the  $r' = \mathbf{0}$  plane of  $\widehat{D}(r', \rho')$  is first used to obtain  $\widehat{\Psi}(\rho')$  within the circle of radius  $\alpha$  labelled  $C_0$ . Next, the  $r' = \beta$  plane of  $\widehat{D}(r', \rho')$ , together with the value of  $\widehat{\Psi}(\beta)$  just computed, can then be used to obtain  $\widehat{\Psi}(\rho')$

within the circle of radius  $\alpha$  centred at  $\rho' = \beta$ , labelled  $C_\beta$ . Similarly, the  $r' = \gamma$  plane of  $\widehat{D}(r', \rho')$  and  $\widehat{\Psi}(\gamma)$  can then be used to obtain  $\widehat{\Psi}(\rho')$  within the circle  $C_\gamma$ , and so on. In practice, there will of course always be some value of  $\|\rho'\|$ , which will depend on the accuracy to which  $\widehat{D}(r', \rho')$  has been estimated, beyond which  $\widehat{\Psi}(\rho')$  will cease to have meaningful value. Note, however, that due to the redundancy of  $\widehat{D}(r', \rho')$ , there is great scope for improving  $\widehat{\Psi}(\rho')$  by least-squares-type techniques. Consider the value of  $\widehat{\Psi}(\rho')$  at the point  $\rho' = \epsilon$  on fig. 1. Two estimates of this value can be obtained, one from each of the  $r' = \beta$  and  $r' = \delta$  planes of  $\widehat{D}(r', \rho')$ , but there are of course many other possible routes by which values of  $\widehat{\Psi}(\epsilon)$  may be estimated.

### 3. Experimental apparatus

The optical STEM analogue used to obtain the microdiffraction data-sets, shown schematically in fig. 2, is now described. A spatially filtered and collimated He-Ne laser beam ( $\lambda = 640$  nm) is directed onto an aperture of adjustable diameter, followed by a lens ( $f = 310$  mm), which forms a crossover (i.e. probe) at the specimen plane. The specimen is mounted on the scanned stage of a novel scanning optical microscope (interfaced to a Sun SPARC 4 computer), to allow scanning of the specimen with respect to the fixed probe. A CCD camera (EEV P43610, 570 lines  $\times$  350 pixels, positioned 125 mm from the specimen plane) records the microdiffraction patterns, which are digitised to 8 bits by an Imaging Technology Series 151 image processor.

In the examples presented in this paper, the specimen is scanned over a square grid (comprising either  $32 \times 32$  or  $50 \times 50$  positions), the grid

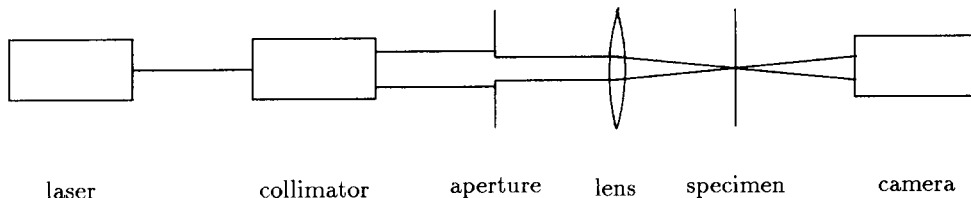


Fig. 2. The optical analogue of a STEM, from which microdiffraction data-sets are obtained.

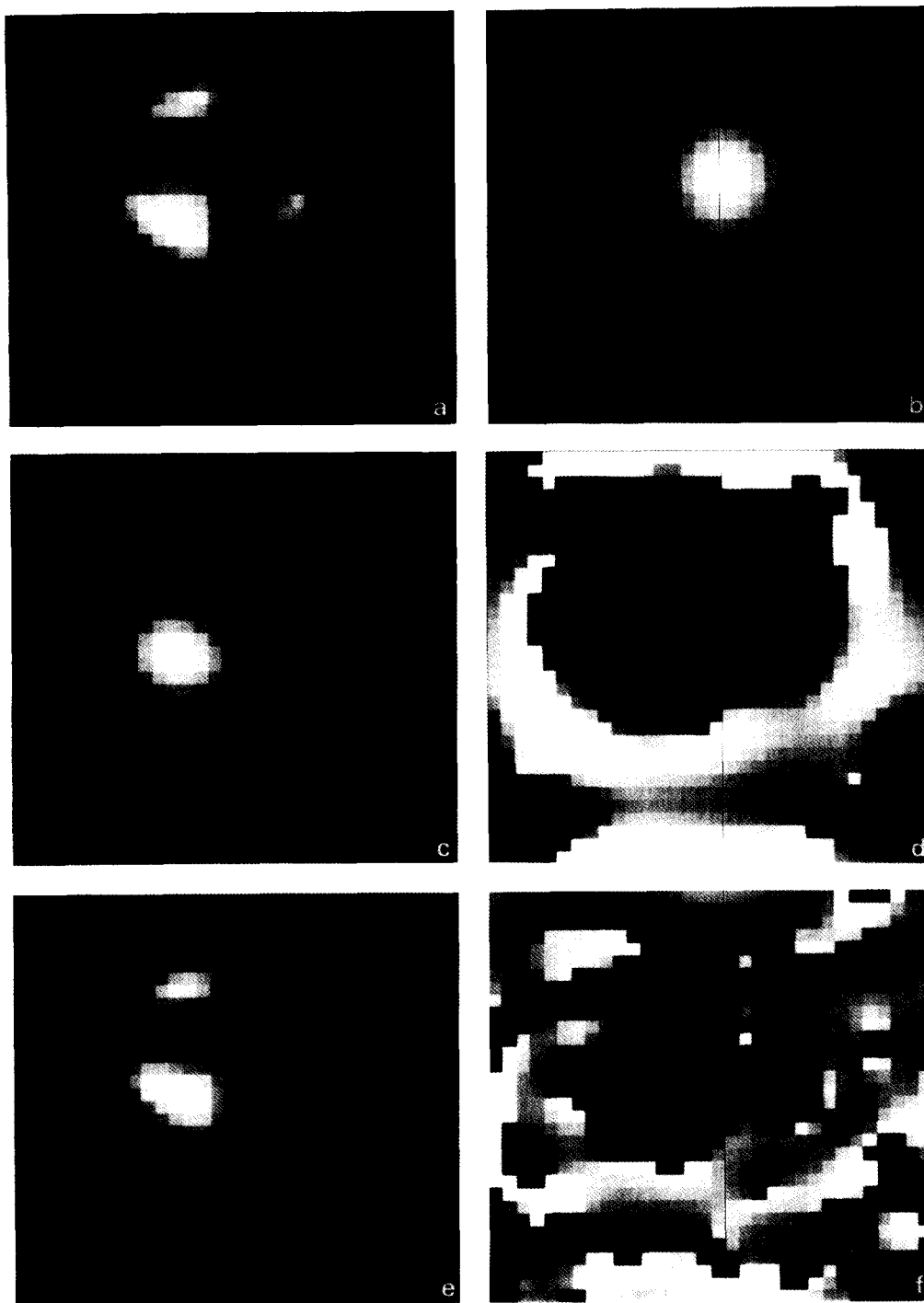


Fig. 3. Reconstruction of a 2D specimen: (a) square-root of bright-field image for 8 mm aperture, (b) bright-field image for 2 mm aperture, (c) magnitude and (d) phase of  $\hat{\psi}(\rho)$  reconstructed to the  $\rho'$  cutoff, (e) magnitude and (f) phase of  $\hat{\psi}(\rho)$  reconstructed to twice the  $\rho'$  cutoff.

spacing being  $12.5 \mu\text{m}$  in each direction. Each microdiffraction pattern is reduced to  $32 \times 32$  samples, spaced by  $0.2 \text{ mm}$  (equivalent to a reciprocal space sampling of  $2.5 \times 10^3 \text{ m}^{-1}$ ).

#### 4. Reconstruction of a 2D amplitude specimen

The first example simply serves to confirm that WPM can be successfully applied to 2D measured microdiffraction data. A suitable specimen was formed by placing a  $200 \mu\text{m}$  electron microscope aperture upon a copper grid specimen mount, both being glued to a glass microscope slide. Initially, a small probe was formed with the adjustable objective aperture set to  $8 \text{ mm}$  diameter, giving a probe of  $13 \text{ mrad}$  half-angle. With this probe, a bright-field image (i.e.  $|M(\mathbf{0}, \boldsymbol{\rho})|^2$ ) was collected, the square-root of which is shown in fig. 3a. We choose to display  $|M(\mathbf{0}, \boldsymbol{\rho})|$  so as to allow comparison with the magnitude of the reconstructed image. Note that all magnitude images are displayed on a linear grey-scale ranging from 0 to a normalised value of 1. Next, a complete microdiffraction data-set (i.e.  $|M(\mathbf{r}', \boldsymbol{\rho})|^2$ ) was collected using a wider probe ( $2 \text{ mm}$  diameter objective aperture). The bright-field image obtained from this data-set is shown in fig. 3b; note that the individual parts of the specimen are no longer resolved.

WPM is applied to this latter data-set, in which  $\chi_a(\mathbf{r}, -\boldsymbol{\rho}')$  is formed by assuming an  $A(\mathbf{r}')$  which is unity within a  $2 \text{ mm}$  diameter circle. The magnitude and phase of  $\widehat{\psi}(\boldsymbol{\rho})$ , obtained by reconstructing to the  $\boldsymbol{\rho}'$  cutoff, are shown in figs. 3c and 3d (displayed on a linear grey-scale ranging from  $-\pi$  to  $\pi$ ), respectively. The resolution of  $\widehat{\psi}(\boldsymbol{\rho})$  is significantly higher than that of the bright-field image, as is to be expected for the reason given in section 2. Since the specimen is pure amplitude, we should expect the phase of  $\widehat{\psi}(\boldsymbol{\rho})$  to be constant at all values of  $\boldsymbol{\rho}$  for which  $|\widehat{\psi}(\boldsymbol{\rho})|$  is significant, as is the case in fig. 3d (note that the phase of  $\widehat{\psi}(\boldsymbol{\rho})$  is meaningless at values of  $\boldsymbol{\rho}$  for which  $|\widehat{\psi}(\boldsymbol{\rho})|$  is small; i.e. in regions of darkness in fig. 3c we expect random phase in fig. 3d).

The magnitude and phase of the reconstruction to twice the  $\boldsymbol{\rho}'$  cutoff (i.e. up to  $\|\boldsymbol{\rho}'\| = 4\alpha$ ) is shown in figs. 3e and 3f. For this case, the reconstruction is performed as follows.  $\widehat{\Psi}(\boldsymbol{\rho}')$  is first reconstructed up to the  $\boldsymbol{\rho}'$  cutoff. Next,  $\boldsymbol{\beta}$  is set to the value of  $\boldsymbol{\rho}'$  at which  $\widehat{\Psi}(\boldsymbol{\rho}')$  has the largest value, giving an estimate of  $\Psi(\boldsymbol{\rho}')$  (call it  $\widehat{\Psi}(\boldsymbol{\rho}')$ ) over the region  $\|\boldsymbol{\rho}' - \boldsymbol{\beta}\| < 2\alpha$ . Any pixel of  $\widehat{\Psi}(\boldsymbol{\rho}')$  in this region whose value has not already been set is then set to the value of the corresponding pixel in  $\widehat{\Psi}(\boldsymbol{\rho}')$ . This process is repeated for the next largest value in  $\widehat{\Psi}(\boldsymbol{\rho}')$ , until all pixels of  $\widehat{\Psi}(\boldsymbol{\rho}')$  in the region  $\|\boldsymbol{\rho}'\| < 4\alpha$  have been set.

#### 5. Reconstruction of an extended amplitude specimen

In any real experiment, it is only possible to measure microdiffraction data from a limited number of probe positions. Thus if WPM is to be applicable to actual STEM data, it must be capable of operating on data measured from a limited region of the specimen. We now show that this is indeed possible.

Consider a microdiffraction data-set in which every microdiffraction pattern is set to zero for values of  $\boldsymbol{\rho}$  outside some region of  $\boldsymbol{\rho}$ -space. This can be achieved by multiplying the measured microdiffraction data-set by a windowing function  $w(\boldsymbol{\rho})$  (which should fall smoothly to zero at its edges), giving rise to a "reduced microdiffraction data-set"  $R(\mathbf{r}', \boldsymbol{\rho})$  as

$$R(\mathbf{r}', \boldsymbol{\rho}) = w(\boldsymbol{\rho}) |M(\mathbf{r}', \boldsymbol{\rho})|^2. \quad (10)$$

If  $w(\boldsymbol{\rho})$  satisfies

$$w(\boldsymbol{\rho}) = v(-\boldsymbol{\rho})v^*(-\boldsymbol{\rho}), \quad (11)$$

then  $R(\mathbf{r}', \boldsymbol{\rho})$  can be written (using eq. (3)) as

$$\begin{aligned} R(\mathbf{r}', \boldsymbol{\rho}) &= \int \int a(\mathbf{b})v(-\boldsymbol{\rho})\psi(\mathbf{b}-\boldsymbol{\rho})a^*(\mathbf{c})v^*(-\boldsymbol{\rho}) \\ &\quad \times \psi^*(\mathbf{c}-\boldsymbol{\rho}) \exp[i2\pi(\mathbf{b}-\mathbf{c}) \cdot \mathbf{r}'] \, d\mathbf{b} \, d\mathbf{c}. \end{aligned} \quad (12)$$

If the value of  $w(\mathbf{r})$  does not vary considerably over the region in which  $a(\mathbf{r})$  has a significant value, then

$$R(\mathbf{r}', \boldsymbol{\rho}) \approx \iint a(\mathbf{b})v(\mathbf{b}-\boldsymbol{\rho})\psi(\mathbf{b}-\boldsymbol{\rho})a^*(\mathbf{c})v^*(\mathbf{c}-\boldsymbol{\rho}) \times \psi^*(\mathbf{c}-\boldsymbol{\rho}) \exp[i2\pi(\mathbf{b}-\mathbf{c}) \cdot \mathbf{r}'] d\mathbf{b} d\mathbf{c}. \quad (13)$$

Comparison with eq. (3) indicates that

$$R(\mathbf{r}', \boldsymbol{\rho}) \approx |\text{FT}_{\mathbf{r}}\{a(\mathbf{r}-\boldsymbol{\rho})\psi_w(\mathbf{r})\}|^2, \quad (14)$$

where

$$\psi_w(\mathbf{r}) = v(\mathbf{r})\psi(\mathbf{r}). \quad (15)$$

Thus when WPM is applied to a reduced microdiffraction data-set (as defined by eq. (10)), it simply reconstructs a windowed version of the extended specimen function (provided that  $w(\boldsymbol{\rho})$  effectively satisfies the condition mentioned above).

This scheme is now applied to measured optical microdiffraction data. An extended specimen was fabricated by mounting three copper grid specimen mounts at different orientations on a

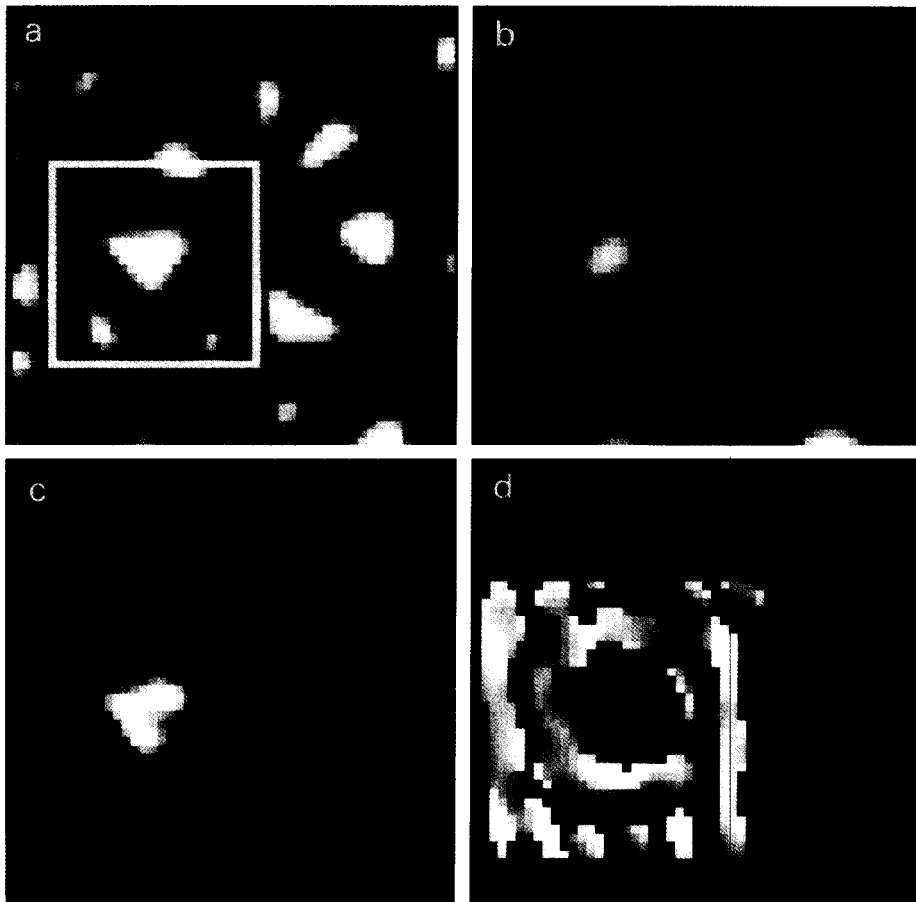


Fig. 4. Reconstruction of an extended specimen: (a) square-root of bright-field image for 8 mm aperture, (b) bright-field image for 2 mm aperture, (c) magnitude and (d) phase of  $\widehat{\psi}(\boldsymbol{\rho})$  reconstructed to twice the  $\boldsymbol{\rho}'$  cutoff for 2 mm aperture, using only data corresponding to values of  $\boldsymbol{\rho}$  within the square superimposed on (a).

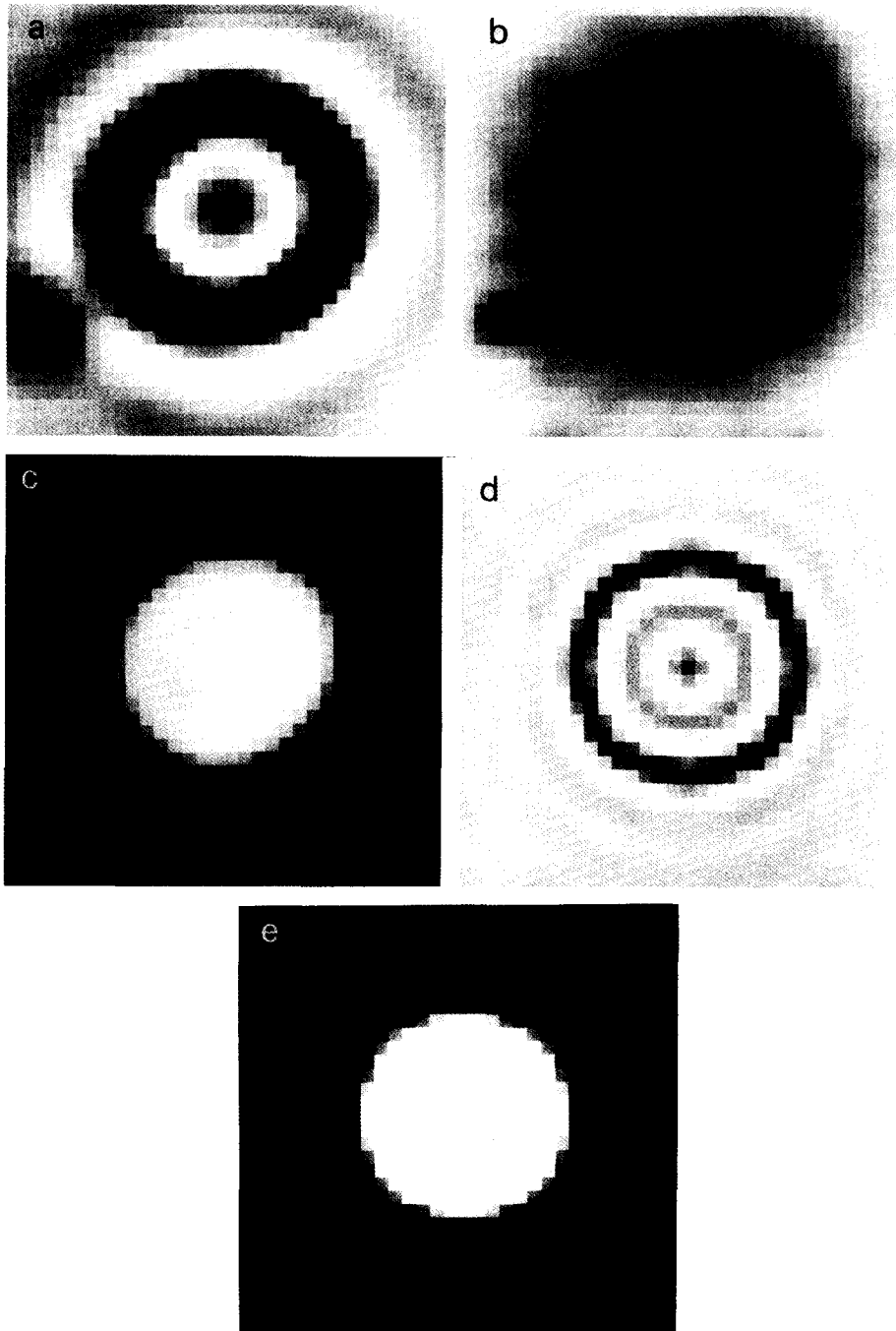


Fig. 5. Reconstruction of a phase specimen: (a) bright-field image for 4 mm aperture, (b) magnitude and (c) phase of  $\widehat{\psi}(\rho)$  reconstructed to the  $\rho'$  cutoff, (d) magnitude and (e) phase of modelled specimen function, diffraction-limited by 8 mm aperture.

glass microscope slide. Fig. 4a shows the square-root of the  $50 \times 50$  pixel bright-field image obtained with a tight probe (8 mm diameter objective aperture). A data-set was then collected with a wide probe (2 mm diameter objective aperture), the bright-field image of which is shown in fig. 4b. A smooth window function was applied to this  $|M(\mathbf{r}', \boldsymbol{\rho})|^2$ , which reduced all pixels to zero for values of  $\boldsymbol{\rho}$  outside the  $22 \times 22$  pixel square superimposed upon fig. 4a. The magnitude and phase (displayed on a linear grey-scale ranging from  $-\pi$  to  $\pi$ ) of the reconstructed specimen function are shown in figs. 4c and 4d, respectively.

## 6. Reconstruction of a pure phase specimen

WPM can in principle be employed to image phase specimens, since it recovers the complex amplitude of the specimen function. It is now shown that this is indeed possible with measured microdiffraction data.

A pure phase specimen with known phase variation was required, so that it could be demonstrated that WPM can successfully reconstruct the specimen phase. A suitable specimen was constructed by evaporating a layer of borosilicate of approximately 470 nm thickness onto a glass microscope slide. A copper specimen mount with a 200  $\mu\text{m}$  diameter hole was used as a mask, which was removed after evaporation, thereby leaving a transparent disc on the glass substrate. The phase delay introduced to a beam passing through this disc relative to one passing outside the disc is approximately  $2\pi/3$ . It should be pointed out that a weak-phase approximation is not valid for this specimen, our intention being to show that WPM is also applicable to strong-phase specimens.

With the specimen described above, a data-set was collected with a 4 mm objective aperture. The bright-field image obtained from this data-set is shown in fig. 5a. Note the appreciable contrast in the bright-field image, despite the imaging lens being at Gaussian focus, due to the specimen not being weak-phase. Figs. 5b and 5c show the magnitude and phase (displayed on a linear grey-scale

ranging from  $-0.4$  to  $2.1$ ) of the reconstructed  $\widehat{\psi}(\boldsymbol{\rho})$ , reconstructed up to the  $\boldsymbol{\rho}'$  cutoff. The value of the phase of  $\widehat{\psi}(\mathbf{r})$  across the disc is approximately 1.9 relative to the background. This compares favourably with the expected value of  $2\pi/3$ .

It is informative to compare the reconstructed  $\widehat{\psi}(\boldsymbol{\rho})$  with the expected reconstruction, which is possible in this case since the original specimen function is known. As explained in section 2, the ideal  $\widehat{\psi}(\boldsymbol{\rho})$  obtained when reconstructing up to the  $\boldsymbol{\rho}'$  cutoff is simply the specimen function diffraction-limited to twice the diameter of the objective aperture in reciprocal space. Figs. 5d and 5e show, respectively, the computed magnitude and phase (displayed on the same grey-scale as fig. 5c) of a specimen function modelling the specimen used in the above experiment, after being diffraction-limited to a diameter equivalent to an 8 mm objective aperture in reciprocal space. Note the similarity between figs. 5e and 5c. Fig. 5d, which has considerable contrast because the specimen is not weak-phase, has a form similar to fig. 5b, the differences being due to the effects of the Wiener filter used to form  $\widehat{\chi}_{\psi}(\mathbf{r}, \boldsymbol{\rho}')$  (as described in section 2) and noise on the measured data.

## 7. Conclusions

WPM promises to overcome the resolution limit in the transmission electron microscope by relatively cheap and experimentally straightforward means. All that is required is to collect a set of coherent electron microdiffraction patterns in the STEM from many probe positions, and perform the recipe described above. Alternatively, a set of conventional images recorded at a number of beam tilt angles could provide a similar data set from a conventional transmission electron microscope (CTEM). However, testing this scheme in the electron microscope for specimens which are not crystalline will not be easy, if only because the resulting image cannot be compared with any known data. For example, if we obtained a sub-ångström resolution image of an amorphous material, how can we trust the recon-

structured solution if it shows detail that has never been seen before and which cannot be tested independently? The experiments described above have served to show that insofar as electron scattering is analogous to light scattering, the WPM inversion method is computationally sound and robust for two-dimensional images. Of course, in the electron case we will face much greater difficulties: the specimen may contaminate, damage or drift during the data acquisition time; the scattering may not fulfill the projection approximation we assume here; the illumination may not be sufficiently coherent, even when a field-emission gun is used. We are confident, though, that the processing method can be relied upon, and so it would now be timely to apply the technique to the STEM.

### **Acknowledgements**

The authors would like to thank Harald Müllejans, Andrew Bleloch and Dennis McMul-

lan for assistance with the scanning optical microscope, and Mary Cluckie and David Wallis for help with specimen preparation. The financial support of the New Zealand (B.McC.) and London (J.M.R.) Royal Societies, and the Science and Engineering Research Council, is gratefully acknowledged.

### **References**

- [1] J.M. Cowley, *Adv. Electron. Electron Phys.* 46 (1978) 1.
- [2] J.M. Cowley, *Ultramicroscopy* 4 (1979) 435.
- [3] D. Gabor, *Nature* 161 (1948) 777.
- [4] J.A. Lin and J.M. Cowley, *Ultramicroscopy* 19 (1986) 179.
- [5] R.H.T. Bates and J.M. Rodenburg, *Ultramicroscopy* 31 (1989) 303.
- [6] J.M. Rodenburg and R.H.T. Bates, *Phil. Trans. A* 339 (1992) 521.
- [7] J.M. Cowley, *Appl. Phys. Lett.* 15 (1969) 58.
- [8] L. Cohen, *Proc. IEEE* 77 (1989) 941.
- [9] R.H.T. Bates and M.J. McDonnell, *Image Restoration and Reconstruction* (Clarendon, Oxford, 1986).